NASA Technical Memorandum 84901

REAL-TIME FLUTTER ANALYSIS OF AN ACTIVE FLUTTER-SUPPRESSION SYSTEM ON A REMOTELY PILOTED RESEARCH AIRCRAFT

Glenn B. Gilyard and John W. Edwards

January 1983

NASA

NASA Technical Memorandum 84901

REAL-TIME FLUTTER ANALYSIS OF AN ACTIVE FLUTTER-SUPPRESSION SYSTEM ON A REMOTELY PILOTED RESEARCH AIRCRAFT

Glenn B. Gilyard
Ames Research Center
Dryden Flight Research Facility
Edwards, California

and

John W. Edwards
Langley Research Center
Hampton, Virginia

National Aeronautics and
Space Administration

1983

REAL-TIME FLUTTER ANALYSIS OF AN ACTIVE FLUTTER-SUPPRESSION SYSTEM ON A REMOTELY PILOTED RESEARCH AIRCRAFT

Glenn B. Gilyard
NASA Ames Research Center
Dryden Flight Research Facility
P.O. Box 273
Edwards, California 93523, U.S.A.

John W. Edwards
NASA Langley Research Center
Hampton, Virginia 23665, U.S.A.

SUMMARY

Flight flutter-test results of the first aeroelastic research wing (ARW-1) of NASA's drones for aerodynamic and structural testing (DAST) program are presented. The flight-test operation and the implementation of the active flutter-suppression system are described. The software techniques used to obtain real-time damping estimates and the actual flutter testing procedure are also described in detail. Real-time analysis of fast-frequency aileron excitation sweeps provided reliable damping estimates. The open-loop flutter boundary was well defined at two altitudes; a maximum Mach number of 0.91 was obtained. Both open-loop and closed-loop data have been of exceptionally high quality. Although the flutter-suppression system provided augmented damping at speeds below the flutter boundary, an error in the implementation of the system resulted in the system being less stable than predicted. The vehicle encountered system-on flutter shortly after crossing the open-loop flutter boundary on the third flight and was lost. The aircraft has been rebuilt, and initial testing is scheduled for the fall of 1982. Changes made in real-time test techniques are included.

SYMBOLS AND ABBREVIATIONS

ARW-1	aeroelastic research wing no. 1	PCM	pulse code modulation
ARW-1R	aeroelastic research wing no. 1, rebuilt	RPRV	remotely piloted research vehicle
a_z	normal acceleration, g	s	Laplace transform variable, rad/sec
CMP	control and monitor panel	S_{xx}	auto-spectrum of x
$d\varphi/d\omega$	rate of change of phase, deg/deg	S_{xy}	cross-spectrum between x and y
DAST	drones for aerodynamic and structural testing	t, T	time, sec
f	frequency, Hz	u	intermediate FSS variable
F	Fourier transform	α	angle of attack, deg
FSS	flutter-suppression system	δ, δ_a	aileron position, deg
G_c	common filter-transfer function	ζ	damping ratio
G_s, G_a	symmetric and antisymmetric filter-transfer functions	σ	$\zeta\omega$
GVT	ground vibration test	$\ddot{\varphi}$	center-of-gravity roll acceleration, rad/sec^2
H	altitude, m (ft)	ω	frequency, rad/sec
$H(s)$	single-degree-of-freedom transfer function	Subscripts:	
i	-1	c	command variable
K	FSS gain	cg	center of gravity
M	Mach number	l, r	left, right
M_f	flutter Mach number	s, a	symmetric, antisymmetric
		tm	tip mass

1.0 INTRODUCTION

Correlation of theoretical predictions and experimental flight-test results of aeroelastic effects in the high subsonic to transonic speed range are of great interest because aeroelastic effects frequently are critical in aircraft design. An objective of NASA's drones for aerodynamic and structural testing (DAST) program (Ref. 1) is to pursue investigations within this speed range, using a series of aeroelastic research wings (ARW) which will be flight tested in combination with a modified Firebee II target drone vehicle fuselage utilizing the remotely piloted research vehicle (RPRV) technique (Ref. 2). DAST is a joint program of Langley Research Center and the

Dryden Flight Research Facility, Ames Research Center. The flight tests described in this paper were supported under contract by the Boeing Military Aircraft Company, Wichita Division. The first wing to be tested in the DAST program, denoted the ARW-1, is a sweptback, supercritical airfoil, transport-type wing with a performance design point of $M = 0.98$ at 13.72 km (45,000 ft).

The primary research objective of the ARW-1 is to investigate, through flight test, those systems synthesis and analysis techniques applicable to active control of flutter, utilizing an on-board analog flutter-suppression system (FSS). A secondary objective is to use flight test to validate analysis techniques for aerodynamic loads predictions. The use of the RPRV technique poses special considerations in the conduct of the flight testing, because test time per flight is quite limited and a higher probability of vehicle loss can be an accepted risk. As such, the flight testing of the ARW-1 had the additional objective of developing flutter-test techniques for use under these conditions.

This paper presents details of the flutter-test technique development and of the implementation of the FSS on the vehicle. Frequency and damping estimates obtained from flight tests using this real-time estimation technique are compared with predictions from Ref. 3. Newsom and Pototsky (Ref. 3) present details of the mathematical modeling and FSS design, and Bennett and Abel (Ref. 4) present more detailed frequency and damping estimates obtained using a postflight parameter-estimation technique. Three operational flights of the ARW-1 were conducted.

Because of an error in the implementation of a gain in the FSS, the vehicle experienced flutter on the third flight; the flutter caused the right wing to separate and there was further damage caused by ground impact. The aircraft has been rebuilt and is approaching a new phase of flight testing. Improvements made in the real-time flutter-test techniques are included in this paper.

2.0 DAST SYSTEM DESCRIPTION

The first wing to be tested in the DAST program is a 6.8 aspect ratio, sweptback, transport-type wing with a supercritical airfoil shape. Design of this wing and the active flutter-suppression system is described in Refs. 1 and 5. Although the supercritical wing design point was at $M = 0.98$ and $H = 13.72$ km (45,000 ft), the achievement of the active flutter-suppression experiment goal of a 20% increase over the unaugmented flutter speed was to be accomplished at altitudes of only 3.05-4.57 km (10,000-15,000 ft). The basic Firebee drone has no wing control surfaces; it is controlled by deflections of the collective and differential horizontal stabilizer and rudder. The ARW-1 retained this method of flight control, thus leaving the wing ailerons free to perform the flutter-suppression fuction.

Figure 1 shows the overall planform of the vehicle. The wing was constructed with front and rear steel spars, with torsional stiffness provided by fiberglass skins. The wing leading and trailing edges are constructed of fiberglass; the wing span is 4.30 m (14 ft). To produce wing flutter within the operational envelope of the vehicle, torsional stiffness was intentionally reduced by orienting the fiberglass filaments at 0° and 90° to the front spar. During wing fabrication, it became apparent that the torsional stiffness was higher than predicted, resulting in a predicted flutter boundary at a higher Mach number than desired. To reduce the flutter Mach number, 0.91 kg (2 lb) of wingtip ballast (encapsulated lead shot) was added.

2.1 Tip-Mass Release System

Automatic or manual jettison of the tip masses was viewed as a desirable feature in order to aid recovery from inadvertent large-amplitude wing oscillations. This was accomplished on the ARW-1 by sensing wingtip accelerations and firing a pyrotechnic device to allow the lead-shot ballast to be thrown out of its container. The automatic firing sequence was initiated when the rms wingtip acceleration exceeded a 10.6-g threshold, with the actual firing occurring after a delay determined by the rms acceleration level in excess of the threshold. For instance, a sinusoidal wingtip oscillation of ±15 g's (10.6 g's rms) at 20 Hz would cause tip-mass firing after 12 cycles of oscillation, and an amplitude of ±30 g's would release the masses after 3 cycles. The threshold g-level was selected based on the acceleration causing saturation of the FSS compensator. It was predicted that structural failure of the wing would not occur until wingtip accelerations reached 64 g's and that compressive stress of the wing skin along the 25% chord line was the critical stress. It was anticipated that this automatic tip-mass release system could save the wing structure in event of mildly divergent wing oscillations. A backup manual tip-mass release capability was provided for the flutter-test experimenters for activation at their discretion. Reference 1 describes a wind-tunnel test of this tip-mass release technique in which a solid weight was manually released at the open-loop flutter boundary when mildly divergent oscillations were observed. The wing response changed quickly to stable convergent oscillations, indicating an incremental increase in damping.

2.2 Mathematical Model

A NASTRAN finite-element model of the ARW-1 and Firebee fuselage-empennage was constructed and ground vibration tests (GVT) were performed on the vehicle. Table 1 presents comparisons of the frequencies obtained by NASTRAN and GVT; the results show fair to good agreement between the two. The differences between NASTRAN and GVT in first wing-bending-mode frequencies (0.5 Hz for symmetric and 1.2 Hz for antisymmetric) are larger than desirable; however, attempts to refine the NASTRAN model did not significantly improve the agreement with the GVT results.

Aeroelastic analysis, using a doublet lattice computer program, predicted classical wing bending-torsion flutter in both symmetrical and antisymmetrical modes at nearly identical altitude/Mach number conditions. In both cases, the lower frequency first wing-bending modes near 10 Hz combined with the bending-torsion modes near 30 Hz to produce flutter modes in the range of 15-20 Hz, with the lower frequency bending modes becoming the unstable flutter modes.

2.3 Instrumentation

All on-board data measurements were telemetered to the ground via two pulse-code-modulation (PCM) telemetry systems; there was no on-board recording capability. The critical flutter parameters, such as accelerations, aileron deflections, excitation signal, and servo commands, were transmitted at the maximum rate of 500 sps. All of these signals were analog-prefiltered to prevent aliasing, with most channels incorporating 70-Hz, sixth-order filters. The remaining primary PCM system parameters consisted of 46 signals sampled at 50, 100, and 250 sps comprising a standard flight-test instrumentation lineup. The secondary PCM system (Ref. 6) monitored sensors, installed in the wing, that were devoted to the loads experiment. There were 86 static upper and lower surface pressure sensors and 16 strain gages.

3.0 FLUTTER-SUPPRESSION SYSTEM

The flutter-suppression system (FSS) was designed and fabricated under contract (Ref. 5) and was implemented as an on-board analog system, as shown in Fig. 1. No redundancy was provided for any of the systems' sensors, electronics, or actuators. The 23%-chord ailerons have a 0.254 m (10 in) span and are located just inboard of the wing closure rib. During the FSS design study, combinations of two accelerometers on each wingtip were considered for sensing wing motion, but a single accelerometer mounted on the rear spar at the outboard aileron edge was chosen.

Miniaturized rotary-vane hydraulic actuators (Ref. 7) were used to control the aileron motion. Figure 1 shows the location of the hydraulic pump and accumulator and the electrohydraulic servovalves which were separated from the actuators by 2.14 m (7 ft) of hydraulic tubing. The control surfaces were stabilized with position and differential pressure feedback. The bandwidth of these control surfaces proved to be a critical variable in the FSS design. Preliminary design of the FSS was accomplished assuming a mathematical model of the controls with a bandwidth of 100 Hz. When the controls were fabricated and bench tested, a 70-Hz bandwidth was achieved; when the control surfaces were installed in the wing, the final bandwidth was 50 Hz. The resulting phase lag ($\approx 30°$ at 20 Hz) severely compromised the original FSS compensator design.

Since suppression of both symmetrical and antisymmetrical flutter modes was required, the FSS compensator was implemented by means of the summing and differencing networks shown schematically in Fig. 2. The left and right wingtip accelerations, a_{z_l} and a_{z_r}, were passed through common filters, G_c, and then summed to yield the symmetric intermediate signal, u_s, and differenced to yield the antisymmetric intermediate signal, u_a. In order to isolate the FSS dynamics from the lower-frequency rigid-body dynamics, the center-of-gravity acceleration, $a_{z_{cg}}$, was subtracted from each signal and the fuselage roll acceleration, $\ddot{\varphi}$, was added to a_{z_l} and subtracted from a_{z_r}. The intermediate signals, u_s and u_a, were filtered by G_s and G_a, and the resulting signals summed, differenced, and multiplied by the gain, K, to yield the left and right aileron servo commands δ_{l_c} and δ_{r_c}.

Although predictions indicated that the reduced control-surface bandwidth previously mentioned would not allow achievement of a 20% increase in flutter speed, it was adequate for flutter suppression at speeds moderately above the flutter boundary, and it was retained for the first two flight operations. During this time period, the FSS was redesigned incorporating the reduced bandwidth characteristics of the servoactuator system. This redesigned system was used for the third flight but because of an implementation error, the flight system had one-half the nominal design gain.

Figure 3 presents the predicted performance of the above defined symmetrical FSS, showing the loci of the open-loop bending and bending-torsion modes versus Mach number. The open-loop bending mode goes unstable (flutters) at approximately $M = 0.83$ at a frequency of 100 rad/sec (16 Hz), and the open-loop torsion mode becomes heavily damped as Mach number increases. Also shown, near $\omega = 100$ rad/sec is the locus of the first fuselage bending mode, which indicates considerable coupling with the bending mode near M_f. The effect of increasing the gain from 0.0 to 1.0 is shown for $M = 0.75$, 0.85, and 0.90. Acceptable damping is achieved at all Mach numbers for nominal gain ($K = 1.0$), but the bending mode is predicted to be unstable above $M = 0.85$ at one-half nominal gain. The torsion mode is heavily damped by the FSS at all Mach numbers.

4.0 DAST OPERATIONAL TECHNIQUE

The flight-test operations of the DAST program utilize the RPRV technique developed by Dryden Flight Research Facility (Ref. 2). The Firebee II vehicle with the ARW-1 wing was air-launched from a B-52 aircraft, flew a preplanned flight track and test points, and was recovered in midair by an Air Force helicopter crew. With the ARW-1 wing installed, flight-test time for each flight varied between 15 and 30 min, depending on the flight conditions chosen. The vehicle was remotely controlled from a ground-based RPRV facility consisting of (1) a PCM telemetry downlink receiver and uplink transmitter, (2) a dedicated, simulation-type cockpit from which the test pilot controls the aircraft, and (3) a ground-based computer interfacing the telemetry links and the cockpit and also providing closed-loop remote control augmentation. In the event of loss of the command signal from the ground, a backup controller in an F-104 chase aircraft provides basic attitude control capability via an air-to-air telemetry link.

The telemetry downlink receives the signal from the primary PCM system described earlier, and the telemetry uplink transmits proportional PCM-coded stabilator, rudder, and throttle commands. The computer was programmed to provide the pilot with selectable augmentation modes in the pitch, roll, and yaw axes. Rate-damper, altitude-hold, and attitude-hold modes were provided in the pitch axis. The roll-axis augmentation consisted of roll-damper and bank-angle hold modes, and the yaw-axis augmentation consisted of a yaw damper. These modes were additive and, when flying straight and level, were all engaged. To perform turns, the pilot disengaged the bank-angle hold and selected roll-rate damping. The intent of these augmented modes was to allow the DAST

pilot to control the small, highly responsive Firebee II vehicle and to concentrate maximum attention on Mach number and altitude so that the flutter-test points could be flown with precision. During the flight tests, the pilot was able to maintain the vehicle to within ±0.01 Mach number of the desired test-point conditions.

5.0 FLUTTER-TEST TECHNIQUE

There are two additional ground-based facilities for monitoring and controlling the progress of the flight test: the control room and the spectral analysis facility. The control room contains strip charts for monitoring the vehicle rigid-body stability and control functions and operational functions, radar plot boards for monitoring vehicle flightpath, and communication equipment required to coordinate the aircraft involved in the test. During flight tests, a test pilot is stationed in the control room to serve as flight director. In the past, the flight director was the only person to communicate directly with the test pilot, but this procedure has been modified for the DAST flutter-test operations. Because of the hazardous nature of active flutter control testing, it was recognized that direct communication between the flutter-test engineers and the test pilot was required. The flutter-test monitoring was performed in a separate location, the spectral analysis facility (SAF).

5.1 Spectral Analysis Facility

The spectral analysis facility (SAF) is a dedicated facility designed to perform spectral analysis of a wide range of experiments as well as flutter testing. Figure 4 is a photograph of the SAF as it is configured for testing of the rebuilt ARW-1. The main elements consist of (1) a dedicated PCM decommutation station and patch panel, (2) a minicomputer-based fast Fourier analyzer (HP-5451C), (3) two x-y plotters, (4) a real-time spectral analysis display (SD-335, referred to as a Spectrascope), (5) the DAST control and monitor panel (CMP), (6) strip charts, (7) video cathode ray tube (CRT) displays, and (8) a plotter computer (TI-990).

Six flutter-test engineers are required for real-time flutter clearance: (1) flutter-test conductor, (2) primary FSS analyst, (3) Spectrascope operator, (4) control and monitor panel operator, (5) primary flutter strip-chart observer, and (6) FSS system health monitor. The flutter-test conductor oversees the conduct of the flutter testing and as such is also in direct communication with the RPRV pilot.

The capabilities of the control and monitor panel are (1) FSS on or off, (2) frequency sweep or pulse excitation, (3) symmetric or antisymmetric excitation, (4) low or high excitation, (5) auxiliary filter in or out switch, and (6) tip-mass release switch. In addition, the primary flutter strip-chart observer is provided a pickle switch to remotely jettison the tip masses.

The Spectrascope is used as a "quick-look" instrument, capable of providing real-time spectral estimates of one of 12 preselected parameters. The Spectrascope has selectable bandwidths and is used primarily to look for problem areas other than those associated with the primary flutter frequencies. In this respect, it augments the Fourier analyzer, which is dedicated to the estimation of frequency and damping of the anticipated flutter modes.

Six channels of high-sample-rate data were input to the Fourier analyzer from the PCM station located in the SAF, using the multiplexer preprocessor. The data channels for ARW-1 were three wingtip accelerations, two aileron deflections, and the FSS excitation signal. The Fourier analyzer computes transfer-function responses of the aileron sweep maneuvers from which frequency and damping are estimated. These results are displayed on the CRT unit. The frequency and damping estimates are also summarized on the x-y plotters: one for symmetric modes and one for antisymmetric modes.

The procedure has been automated such that the Fourier analyzer lights a ready light on the CMP. At this point the CMP operator can initiate the next maneuver command, providing flutter clearance has been granted and the aircraft is at proper flight conditions. Once the maneuver is commanded, a trigger signal is sent to the Fourier analyzer to initiate data gathering.

5.2 FSS Excitation

Flight flutter-test techniques (Refs. 8 and 9) have traditionally relied heavily on long-duration testing to obtain random turbulence excited response or on slow-frequency sweeps to obtain quasi-steady-state forced response. The goal in any case is to obtain reliable estimates of critical mode damping to allow flight testing to proceed. The introduction of minicomputer-based Fourier analyzers utilizing fast-Fourier-transform techniques, coupled with the measurement of both the input forcing function (control-surface displacement) and the response (wing acceleration), allows the use of the transfer-function analysis and greatly reduces test time. Quasi-steady-state test methods are no longer necessary, and fast-frequency sweeps were chosen as the preferred method of excitation. The excitation was summed with the FSS feedback signals, allowing the ailerons to be used both to excite the wing and to control the flutter mode. A logarithmic frequency sweep function was implemented as

$$\delta_{a_c} = A \times \sin\left[a \times \omega_0 \times ln\ (a - t)\right]$$

where $a = \omega_1 \times T/(\omega_1 - \omega_0)$ with ω_0 and ω_1 the starting and stopping fequencies and T the sweep duration. Sweep amplitudes, A, of 1° and 2° were available. Since the predicted flutter frequency was near 20 Hz, the starting and stopping frequencies were chosen to be 10 and 40 Hz. A sweep duration of 7 sec was chosen, based on an 8-sec period required for the Fourier analyzer to take 4,096 data points at the maximum rate of 500 samples per second. This allowed 0.5 sec settling time at the start and end of the sweeps for transients to die out. In addition, the sweep-command amplitude was tapered at the beginning and end to eliminate transients (Ref. 10). In addition to the sweeps, a capability to pulse the ailerons was included so that the test engineers could monitor transient reponses. The pulse consisted of a single cycle of a 20-Hz sine wave with an amplitude of either 1.7° or 3.4°. The primary benefit of the pulsing command was to monitor structural damping during periods when changing flight conditions.

5.3 Transfer-Function Smoothing

Because of the limited flight time available for a given flight, as well as the possibility of losing the aircraft during the midair recovery process, efficient use of flight time was critical. Considerable effort was devoted to minimizing the time required for single-mode frequency and damping estimates, thereby minimizing operator interaction.

The real-time method arrived at is diagrammed in Fig. 5 for open-loop analysis. The raw transfer-function estimate of acceleration response to aileron deflection was obtained as the cross-spectrum, $S_{a_z\delta_a}$, divided by the input autospectrum, $S_{\delta_a\delta_a}$. Minimal input power existed outside the range of the frequency sweep; therefore, the transfer function was set to zero below 10 Hz and above 40 Hz. For closed-loop analysis, the FSS excitation is used in place of the aileron deflection.

Normally it is desirable to obtain multiple maneuvers and perform averaging in order to produce reliable transfer-function estimates. A single raw transfer-function estimate quite often will produce poor results because of noise, truncation, and unknown (i.e., turbulence) forcing functions. When averaging is not feasible, ad hoc smoothing techniques are quite often required to enhance the usefulness of the data. In the DAST program, the luxury of multiple maneuvers was not available and therefore, the raw transfer-functions produced were quite rough.

A number of techniques have been investigated for smoothing the raw transfer function, the first of which was application of an exponential window (Ref. 11). Benefits of the exponential window are ease of application and the simple damping correction factor at resonant frequencies. The inverse Fourier transform of the transfer function, F^{-1}, yields an estimate of the impulse-response function. Block multiplication of the impulse response by e^{-t} forces the function to zero and minimizes extraneous effects for large values of t. The Fourier transform of the smoothed impulse response yields the smooth transfer function. The frequency and damping estimates are then made from this transfer function. The exponential window effects representing the raw and smoothed transfer functions of a_z/δ_a from a symmetrical FSS OFF sweep at $M = 0.74$ and an altitude of 4.57 km (15,000 ft) are presented in Figs. 6 and 7. The magnitude and phase of the raw transfer function are presented in Fig. 6; the results of smoothing with the window e^{-t} are in Fig. 7. The lightly damped mode at $f = 13.3$ Hz is wing bending, and the smaller mode near 16 Hz is first vertical fuselage bending. This window was used during the initial ARW-1 testing.

5.4 Damping Estimation

The smooth transfer function is used to estimate the frequency and damping of the dominant resonant peak. Although many techniques for extracting resonant mode characteristics are available, a primary requirement was for a relatively simple, automated, real-time procedure. The technique selected consisted of searching for the peak magnitude of the transfer function and then, at that frequency, determining a damping estimate from the slope of the phase curve. Damping of a single-degree-of-freedom transfer function $H(s)$ where

$$H(s) = \frac{\omega^2}{s^2 + 2\zeta\omega s + \omega^2}$$

is given by

$$\zeta = \frac{-1.0}{\omega\,(d\varphi/d\omega)}$$

where $d\varphi/d\omega$ is the slope of the phase curve at resonance. The frequency of the peak resonance was estimated by means of a least-squares curve fit of a quadratic function to the five points nearest the peak magnitude. For the first three ARW-1 flights, a five-point least-squares curve fit of a cubic function to the phase curve was used. The derivative of the function was then taken to obtain the slope. For well-defined resonances, this five-point cubic fit provided good damping estimates. The real-time frequency and damping estimates are implemented in the Fourier analyzer in a fully automatic mode.

The first two flights of ARW-1 utilized the program with the maximum data block size available in order to obtain the best results possible (block size of 4096, 500 sps). This block size required 15 sec to process each transfer-function estimate and obtain frequency and damping estimates. Postflight data processing indicated that equivalent results could be obtained with a smaller block size and the third flight utilized the program with a block size of 1024 and a sample rate of 100 sps. This reduced the processing time to 5 sec.

The ARW-1 flight testing was accomplished at constant altitude, using preplanned Mach number increments of 0.050 and 0.025. The test procedure at each flight condition depended on whether the flight condition was above or below the predicted open-loop flutter Mach number. At conditions below the flutter boundary, a sequence of four sweeps was used: (1) symmetric, FSS OFF, (2) antisymmetric, FSS OFF, (3) antisymmetric, FSS ON, and (4) symmetric, FSS ON. Beyond the open-loop flutter boundary, the FSS could obviously not be turned off and only the two FSS ON sweeps were to be obtained.

The left and right wing aileron positions and accelerations were summed and differenced to provide signals for symmetric and antisymmetric processing. For FSS OFF tests, transfer functions of acceleration due to aileron motion provided open-loop damping estimates, and transfer functions of acceleration due to the excitation signal provided closed-loop damping estimates for the FSS ON tests. For the FSS ON sweeps, transfer-function

estimates were also obtained for wing acceleration due to aileron motion in an attempt to determine the open-loop damping from closed-loop data. This technique requires that the data be relatively noise-free and also free from extraneous inputs such as atmospheric turbulence.

6.0 FLIGHT TEST RESULTS

It was anticipated that the objectives of the flutter-suppression tests could be accomplished in six flights (Ref. 1). Testing was planned at low, medium, and high altitudes, with the FSS design point to be reached on the fourth flight at 3.05 km (10,000 ft). The first flight was to be devoted to subcritical testing, exercising the FSS at Mach numbers no closer than 0.1 M to the predicted flutter boundary. The second flight was to test 0.05 M past M_f with the FSS engaged. Figure 8 shows the test points that were achieved on the three flights of the ARW-1 and gives the predicted flutter boundaries that were used to plan the third flight. Boundaries are shown for FSS OFF and ON and for the tip masses ON and OFF. The open symbols in Fig. 8 denote test points at which only FSS OFF testing was accomplished, and the half-open symbols indicate test points for both FSS OFF and FSS ON testing. Solid symbols indicate those points that were predicted to be at or above the flutter Mach number, and thus only FSS ON testing was done.

There were several difficulties during the first flight, including failure of the FSS hydraulic pump and intermittent loss of the telemetry uplink command signal; the latter resulted in a premature flight termination.

At the first test point on the second flight (M = 0.7 at 6.10 km (20,000 ft)) a 200-Hz, limited amplitude instability was observed when the FSS was engaged. Similar instabilities had been encountered during ground testing; they were caused by the interaction of the high-bandwidth aileron control systems with the structure. These hydraulic resonances observed during ground testing were controlled with notch filters, and when they were observed in flight it was decided to terminate FSS ON testing for the remainder of the flight, even though the FSS was providing excellent control of the bending modes at the first test point. The flight lasted 25 min and test data were obtained from 14 frequency sweeps and 177 pulses. The flight resulted in a very good definition of the flutter boundary at approximately M = 0.92 and 7.62 km (25,000 ft) (Fig. 8), whereas analysis had predicted M_f = 0.95 at this altitude. This led to the incorporation of a correction factor (Ref. 3) into the unsteady airloads; this factor was based on the ratio of the static rigid-body lift-curve slope measured during a wind-tunnel test to its predicted value. This correction factor was included in the predictions used in the planning of the third flight.

The objective of the third flight was to test 0.05 M past the open-loop flutter boundary at 4.57 km (15,000 ft) and 6.10 km (20,000 ft). Flight planning was based on the more conservative flutter boundary estimated from the first two flights (Fig. 8) rather than the predicted flutter boundary, and M = 0.825 was the highest Mach number to be tested at 4.57 km (15,000 ft). Flight three continued for 10 min before the flutter incident, during which time four test points were achieved and data were obtained from 12 frequency sweeps and 75 pulses.

6.1 Frequency-Sweep Data Analysis

The quality of the flight-test data obtained from the ARW-1 was extremely good. The average rms background acceleration level was approximately 0.25 g's, and responses due to FSS excitation signals ranged up to 10 g's. Consequently, the signal-to-noise ratio was very high. Figure 9 shows time histories of symmetric aileron sweep maneuvers with FSS OFF and FSS ON (low amplitude) at M = 0.74 and at 4.57 km (15,000 ft). Left and right wing-tip accelerations and aileron deflections are presented along with the frequency-sweep excitation. The resonance of the bending mode is clearly seen in the FSS OFF sweep of Fig. 9(a), whereas this mode is heavily damped in the FSS ON sweep of Fig. 9(b). Figure 10 gives the frequencies and dampings obtained during the second flight at 7.62 km (25,000 ft) by the real-time damping estimation technique. The frequencies near 25 Hz are from the more highly damped torsion modes and were determined from postflight analysis. The faired curves through the data points give very good indications of the FSS OFF flutter boundaries between M = 0.91 and 0.92 for both symmetric and antisymmetric modes. Although the solid lines in Fig. 10 are fairings of the real-time data, during the flight the frequency and damping estimates were plotted on graphs containing preplotted predictions.

The elimination of FSS ON testing due to the 200-Hz instability during the second flight left ample flight time for repeat testing at M = 0.85, 0.875, and 0.90; Fig. 10 indicates good repeatability of the damping estimates at these Mach numbers. Also, at M = 0.85, data were obtained from high-amplitude (±2°) frequency sweeps, and the resulting damping estimates shown in Fig. 10 indicate no appreciable amplitude effect at this Mach number. Between the second and third flights, the modified FSS compensator was implemented, including the one-half gain error described earlier. Figure 8 indicates test points at 4.57 km (15,000 ft) and at M = 0.70, 0.75, 0.775, and 0.80, which were achieved before the flutter incident at M = 0.825. The FSS ON nominal gain flutter boundary was predicted to be M_f = 1.06 at this altitude (Fig. 8).

The results of the real-time damping estimates obtained from sweeps on the third flight are presented in Figs. 11 and 12 (root locus plots were not maintained during the actual flutter testing). Comparisons of predictions and flight-test results are shown as s-plane root loci to better explain the effects of FSS OFF and ON and one-half nominal gain. Figure 11 presents the antisymmetric results. The predicted FSS OFF root loci of the bending and torsion modes are shown for $0.70 < M < 0.90$. Also shown are the predictions of the FSS ON dominant mode root loci for nominal and one-half gain. The effect of the FSS on the bending mode is to heavily damp the mode and lower its frequency for Mach numbers less than M_f; the torsion mode is slightly destabilized. Figure 11 indicates that the antisymmetric mode is predicted to be stable, even at one-half gain for Mach numbers up to 0.90. The flight-test frequency and damping estimates are indicated by solid symbols; good agreement with these predictions is apparent. The flight test open-loop bending mode frequencies shown near 100 rad/sec agree well with predictions, although the damping is overpredicted. The flight-test results appear to project to an open-loop flutter boundary at a lower Mach number and frequency than those predicted. The results from the third test point at M = 0.775 are believed to be less reliable than the others, since extraneous wing responses, possibly because of atmospheric turbulence, were observed at this test point. The FSS was kept on for the M = 0.775 and 0.80 cases; therefore, FSS OFF data were calculated from the FSS ON sweep data.

The FSS ON antisymmetric response of the wing correlates well with predictions, as shown by the closed symbols near 160 rad/sec in Fig. 11. Again the $M = 0.775$ result appears to be erratic, and the other three estimates are close to their predicted values, especially at $M = 0.80$. Reference 4 presents frequency and damping estimates of both the bending and torsion modes obtained from postflight analysis, and Ref. 3 gives more details of the predicted response.

Similar information for the symmetric case is presented in Fig. 12. The estimated FSS OFF frequencies and dampings near 80 rad/sec are lower than predicted and project to an open-loop flutter Mach number lower than that predicted. The trend toward instability is in reasonable agreement. As with the antisymmetric case, the results from $M = 0.775$ appear erratic. The effect of the one-half gain error is much more severe in this case, with instability predicted above $M = 0.85$ with FSS ON. Also, the rate of change of damping of the one-half gain locus between $M = 0.825$ and 0.850 indicates a very violent flutter onset, whereas the nominal-gain locus, which was anticipated during the flight, indicates increased damping above $M = 0.825$. The nominal and one-half gain locus have been shown only for the most critical structural mode.

The real-time FSS ON damping estimates for $M = 0.70$ and 0.75 were off scale and are not shown. The more accurate postflight damping estimates of Ref. 4 for these Mach numbers give values of $\zeta \approx 0.13$ and of $\omega \approx 125$ rad/sec, corresponding to a root location at $s \approx 16 \pm i125$ rad/sec, close to the predicted location. Thus, the real-time damping estimation appears to be suspect for damping ratios greater than 0.10. The frequency and damping estimate obtained from the sweep data at $M = 0.80$ and the frequency of the flutter mode at $M = 0.825$ correlate very well with the trend of the predicted one-half gain locus. Particularly interesting is the fact that the doublet-lattice aerodynamic theory predicted the control-surface effectiveness very well. The mathematical model predicted an increase of bending-mode frequency from $\omega = 95$ rad/sec to 131 rad/sec for the one-half gain FSS at $M = 0.80$, whereas the flight data show an increase from 87 rad/sec to 125 rad/sec.

6.2 Pulse Data

Pulse-response data were, in general, obtained at all times except when sweep responses were being measured. Pulse responses were performed in all four possible configurations of FSS OFF or ON and symmetric or antisymmetric; amplitude was also selectable as low or high. The basic requirement for the pulses was to monitor structural damping characteristics by means of the strip chart. Figure 13 is a representative pulse response as observable on the strip chart and was obtained at a symmetric, open-loop configuration of $M = 0.907$ and at 7.62 km (25,000 ft). The pulse data have been analyzed, using postflight techniques to determine their usefulness for providing damping estimates and to study possible angle-of-attack effects on damping at transonic Mach numbers. For the antisymmetric mode, an increase in damping with increasing angle of attack is apparent, as reported in Ref. 12.

6.3 Nyquist Analysis

To gain insight into FSS degradation during the third flight, a postflight Nyquist analysis was performed on the eight FSS ON maneuvers. The maneuvers analyzed consisted of both symmetric and antisymmetric sweeps obtained at Mach numbers of 0.70, 0.74, 0.775, and 0.80. (The Nyquist analysis procedure used is discussed later.) The phase-margin results are presented in Fig. 14; gain-margin results are not presented, because they were not defined over the 10-40-Hz frequency range of interest. The phase-margin results appear to present a clear indication of FSS ON degradation for the symmetric mode. The system design goal had been to provide a minimum 30° margin over the entire FSS ON range. Although preflight predictions indicated the 30° minimum could not be obtained over the entire FSS ON range, the phase-margin results for the symmetric mode at $M = 0.80$ are significantly lower than expected. Although the trends are smooth, the Nyquist analysis of the symmetric sweep at $M = 0.775$ did produce a poor estimate and is the same maneuver referred to earlier as providing a poor (high) damping estimate, which in turn led to the impression the FSS was functioning normally. It should be noted that the Nyquist display of the suspect maneuver was very erratic and, as such, appears to provide a good indication of sweep-response quality.

6.4 Flutter Incident

As the third flight progressed, there was no indication of problems in the operation of the FSS and no warning evident to the flutter-test engineers that the FSS was operating at one-half nominal gain. The FSS ON test results for $M = 0.775$ and 0.80 shown in Figs. 11 and 12 are similar to those anticipated for the full-gain FSS. In particular, the symmetric damping estimate at $M = 0.775$ was misleading, as described above, and had a better estimate been obtained at this Mach number, the trend toward a violent flutter condition would have been apparent at $M = 0.80$. Since the results appeared to agree with the nominal-gain predictions, which indicated a minimum damping condition near $M = 0.80$, clearance was given to $M = 0.825$.

Typical accelerations for Mach increments of 0.025 required from 12 to 15 sec. During the acceleration from $M = 0.80$ to 0.825, several pulse responses were obtained showing increasingly lighter damping. The final pulse that preceded the flutter incident is shown in Fig. 15. Shown are the wingtip FSS accelerometer signals, the wingtip-mass release accelerometer signals, the aileron-position signals, angle of attack, and Mach number. As this pulse response was observed, the test pilot was instructed to terminate the test. The throttle was retarded at the 2.5-sec point, and the motion on the angle-of-attack trace at 3 sec is the result of pilot commands. In the remaining seconds before the flutter incident, however, the Mach number continued to increase. Mildly divergent oscillations at 20 Hz are seen at 3 sec where $M = 0.82$, and rapidly divergent oscillations occur at 4.5 sec where $M = 0.825$. Before the 5-sec point, where the FSS accelerometers go off scale, the oscillations doubled in amplitude in six cycles, corresponding to a negative damping of $\zeta = -0.02$. The ailerons saturated in amplitude two cycles later, followed by the firing of the tip-mass release pyrotechnics at 5.2 sec. (The automatic and manual tip-mass release commands occurred nearly simultaneously.) The saturation of the ailerons resulted in an effective gain reduction and the effect on the wing stability is shown in the $M = 0.85$ gain root locus of Fig. 3. The flutter-mode frequency decreased from 20 Hz to 15 Hz, and the coupling with the 16-Hz fuselage bending mode is apparent in the oscillations seen in the angle-of-attack trace. The rate of growth of the oscillations was so large at the time of the operation of the tip-mass release system that the oscillations were not arrested. Structural failure of the right wingtip and aileron occurred at 5.4 sec followed by failure of the structural attachment of the right wing to the fuselage carrythrough structure at 5.6 sec. The resulting rolling gyrations at large angle of attack and sideslip caused subsequent partial failure of the parachute recovery system and the vehicle hit the ground.

It has been concluded that the primary cause of the flutter incident was the one-half gain setting error in the FSS.

7.0 REBUILT ARW-1

Because of an error in the implementation of the on-board FSS, the ARW-1 encountered flutter on the third test flight and was subsequently lost. At the time of the incident, all systems were functioning and the flutter-suppression techniques applied to the ARW-1 appeared capable of achieving the design goals. Following the incident, a decision was made to rebuild the ARW-1 and complete the flutter-test series to verify the design goals. Although the fuselage structure of the Firebee drone was damaged beyond repair, the wing spars and many of the avionics systems were reusable. The vehicle (referred to hereinafter as ARW-1R) has been rebuilt with some small but important changes.

7.1 Aircraft and Systems Modification

The fiberglass skin of ARW-1 had a significant variation of stiffness versus stress characteristic because of the ply orientation of 0° and 90°. For ARW-1R, some plys are oriented at 45° which produces an improved stiffness versus stress relation (Ref. 13).

An improved tip-mass release system has been designed and implemented for ARW-1R testing. The redesign was required to provide a system that would react to a much more rapid flutter divergence than the previous system. In the new system, there are three ways in which the tip-mass release can be automatically activated: (1) if 2/3 control-surface authority is exceeded, (2) by a 12-g rms level over two cycles, or (3) by a 21-g peak value. Timing windows are used in the logic to minimize any spurious triggering.

An external centerline fuel tank has been added to the vehicle and will at least double flight-test time available. This will also permit a less aggressive testing procedure than was required for the initial vehicle.

The FSS system is being redesigned by Langley Research Center, and the same accelerometer locations and control surfaces will be used. The FSS compensator will require less high-frequency gain than the original system. New actuators have been fabricated which have improved frequency-response characteristics.

7.2 Real-Time Analysis Modifications

In preparing for ARW-1R flight testing, real-time Nyquist plot displays were investigated as a means of providing closed-loop gain and phase-margin information. For this type of data display, the exponential window has a significant shortcoming, in that the phase curve of the smoothed transfer function has a significant negative skew. This effect is observed by comparing the raw phase curve of Fig. 6 with the smooth phase curve of Fig. 7. The result is a rotation of the Nyquist plot which affects gain and phase-margin determination. This effect is due to the asymmetry of the exponential window. Inspection of the impulse response function shows significant (unphysical) information contained in the last half of the record which the exponential window suppresses.

An early ad hoc approach to correcting the dominant effect of this problem requires the addition of a unity pulse at the end of the exponential window (Ref. 10). Although this modified window approach does improve the phase skewing effect, it is not readily applicable in a real-time process, since selection of the unity pulse width is highly data-dependent.

The final smoothing technique arrived at for real-time ARW-1R testing consists of a further refinement in the window modification process. Instead of using a unity pulse at the end of the window, a time-reversed exponential is used. The net window then consists of e^{-t} over the region $t = 0$ to $t = T/2$, and the region from $t = T/2$ to T is a mirror image of the first half. Application of this window eliminates the phase-skew effect of the one-sided exponential window. The effect of this window is illustrated in Fig. 16 for the same a_z/δ_a transfer function of Figs. 6 and 7. The Nyquist analysis requires input of the left and right aileron servovalve position commands to the Fourier analyzer.

For ARW-1R testing, Nyquist results will be displayed in real time and comparisons made with predictions. Maneuver quality will also be evaluated from the Nyquist display.

For well-defined resonances, the five-point cubic fit of the phase curve provided good damping estimates; however, for more poorly defined (i.e., rough) transfer functions, it may produce poor damping estimates, even in some cases with the wrong sign. The main problem is that the curve fit is very sensitive to the data points; this in turn affects the slope determination. For ARW-1R testing, the slope will be determined by a linear fit of the data. This produces a slope less sensitive to any particular data point; however, it will in general produce an unconservative, higher damping estimate, as shown in Fig. 17. The slope estimate will be increasingly unconservative as the number of points used in the curve fit increases. To compensate for the unconservative nature of the estimate, an empirical formula based on a single-degree-of-freedom model, is applied to the damping estimate. It should be noted that the single-sided exponential window will produce a conservative estimate because of the negative phase bias mentioned previously.

8.0 CONCLUDING REMARKS

Flight-test results of the first three flights of an aeroelastic research wing have been described. The flight flutter-test technique used to obtain real-time damping estimates from fast-frequency sweep data was obtained and the open-loop flutter boundary determined. Nyquist analyses of sweep maneuvers appear to provide additional valuable information about FSS operation, both in terms of phase-margin estimates and as a means of evaluating maneuver quality. An error in implementing the flutter-suppression system resulted in a one-half nominal gain configuration, which caused the wing to be unstable at lower Mach numbers than anticipated, and the vehicle experienced closed-loop flutter on its third flight. Real-time flutter-testing procedures have been improved, and ARW-1R testing is scheduled to begin in the fall of 1982.

REFERENCES

1. Murrow, H. N.; and Eckstrom, C. V.: Drones for Aerodynamic and Structural Testing (DAST)—A Status Report. J. Aircraft, vol. 16, Aug. 1979, pp. 521-526.

2. Edwards, J. W.; and Deets, D. A.: Development of a Remote Digital Augmentation System and Application to a Remotely Piloted Research Vehicle. NASA TN D-7941, 1975.

3. Newsom, J. R.; and Pototzky, A. S.: Comparison of Analysis and Flight Test Data for a Drone Aircraft with Active Flutter Suppression. AIAA Paper 81-0640, Atlanta, Ga., 1981.

4. Bennett, R. M.; and Abel, I.: Application of a Flight Test and Data Analysis Technique to Flutter of a Drone Aircraft. AIAA Paper 81-0652, Atlanta, Ga., 1981.

5. Visor, O. W.; and Sevart, F. D.: Preliminary Design Study of Flutter Suppression Control System for BOM-34E/F Drone Aircraft With a Supercritical Wing—Final Report. NASA CR-14508, 1977.

6. Eckstrom, C. V.: Loads Calibration of Strain Gage Bridges on the DAST Project Aeroelastic Research Wing (ARW-1). NASA TM-81889, 1980.

7. Bergmann, G. E.; and Sevart, F. D.: Design and Evaluation of Miniature Control Surface Actuation Systems for Aeroelastic Models. J. Aircraft, vol. 12, Mar. 1975, pp. 129-134.

8. Flutter Testing Techniques. NASA SP-415, 1976.

9. van Nunen, J. W. G.; and Piazzoli, G.: Aeroelastic Flight Test Techniques and Instrumentation, Vol. 9. AGARD Flight Test Instrumentation Series, AGARD-AG-160, Feb. 1979.

10. Jennings, W. P.; Olsen, N. L.; and Walter, M. J.: Transient Excitation and Data Processing Techniques Employing the Fast Fourier Transform for Aeroelastic Testing. Flutter Testing Techniques, NASA SP-415, 1976.

11. Newman, K. W.; Skingle, C. W.; and Gaukroger, D. R.: The Development of Rapid-Testing Techniques for Flutter Experiments. ARC CP No. 1274, 1974.

12. Edwards, John W.: Flight Test Results of an Active Flutter Suppression System Installed on a Remotely Piloted Research Vehicle. AIAA Paper 81-0655, Atlanta, Ga., 1981.

13. Eckstrom, C. V.; and Spain, V.: Design Considerations and Experiences in the Use of Composite Material for an Aeroelastic Research Wing. NASA TM-83291, 1982.

TABLE 1.—NORMAL-MODE FREQUENCIES PREDICTED BY NASTRAN ANALYSIS AND MEASURED DURING GROUND VIBRATION TEST

Mode	Frequency, Hz	
	NASTRAN	GVT
Symmetric—		
First wing bending	9.1	9.6
First fuselage bending	16.5	16.2
Wing bending-torsion	29.6	29.1
Antisymmetric—		
First wing bending	12.3	13.5
First fuselage yaw	21.7	19.3
Wing bending-torsion	30.0	27.0

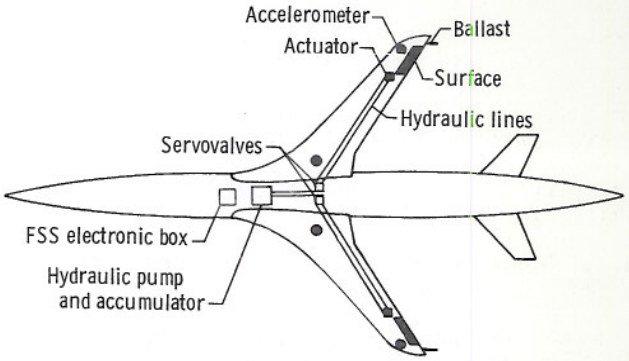

Figure 1. DAST ARW-1/1R planform illustrating the flutter-suppression system layout.

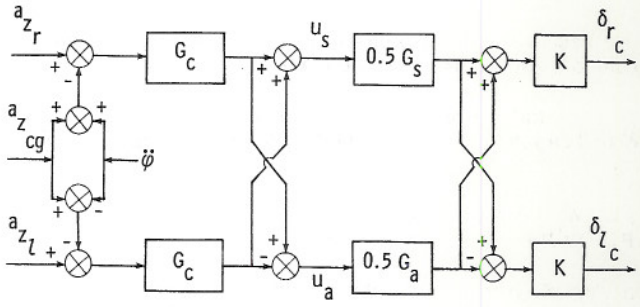

Figure 2. Flutter-suppression system block diagram.

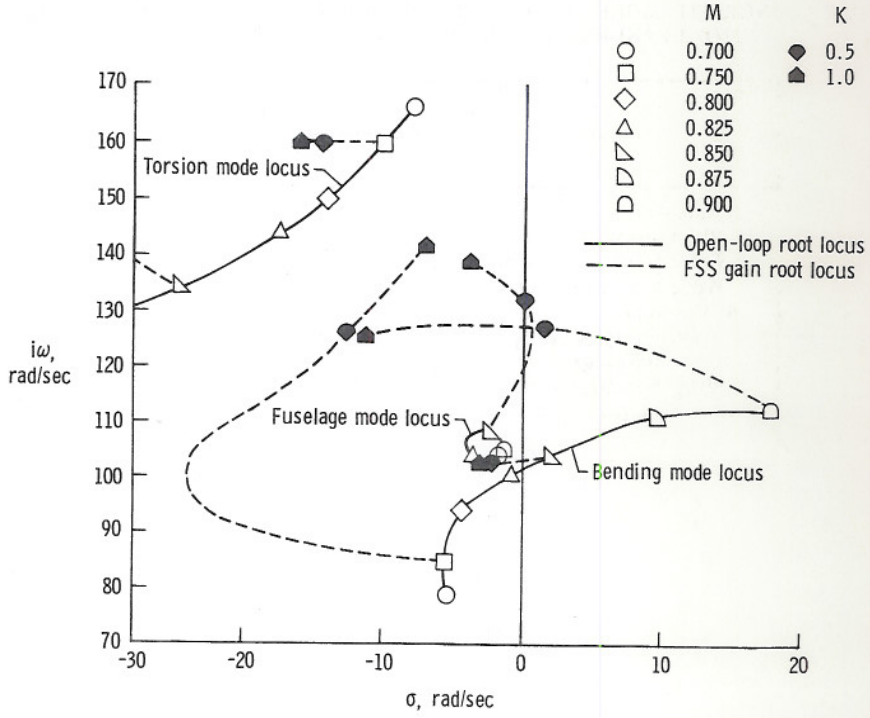

Figure 3. Predicted open-loop flutter-mode root locus and flutter-suppression system gain root locus at H = 4.57 km (15,000 ft).

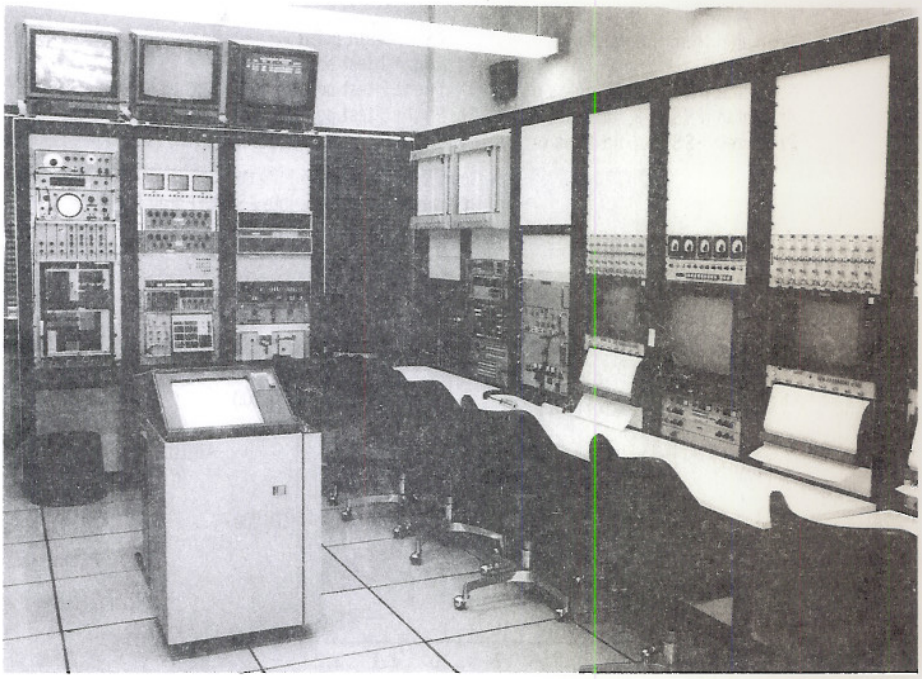

ECN 18946

Figure 4. Spectral analysis facility.

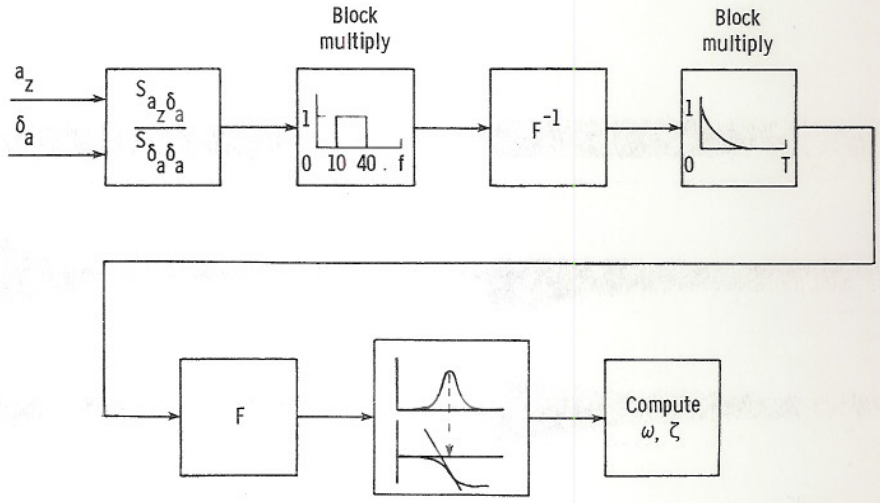

Figure 5. Functional diagram of the real-time transfer-function and damping-ratio estimation algorithm.

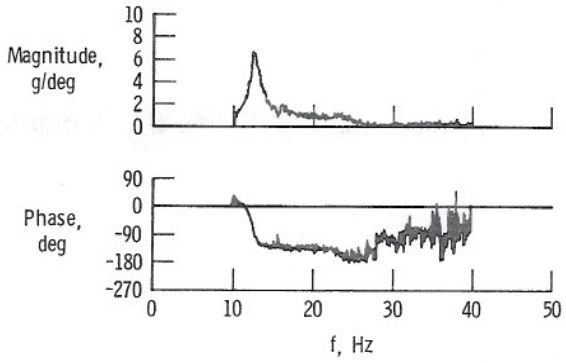

Figure 6. Raw transfer-function estimate of a_z due to δ_a for a symmetrical frequency sweep: M = 0.74 and H = 4.57 km (15,000 ft).

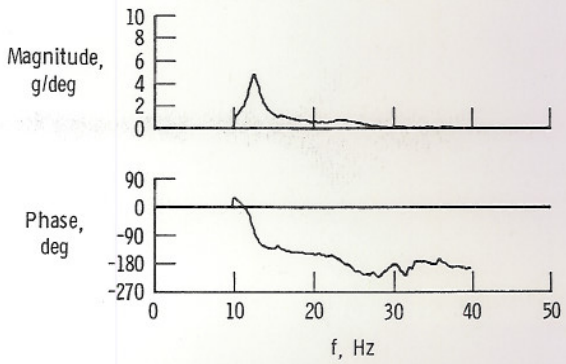

Figure 7. Smoothed transfer-function estimate of a_z due to δ_a for a symmetrical frequency sweep using an exponential window: M = 0.74 and H = 4.57 km (15,000 ft).

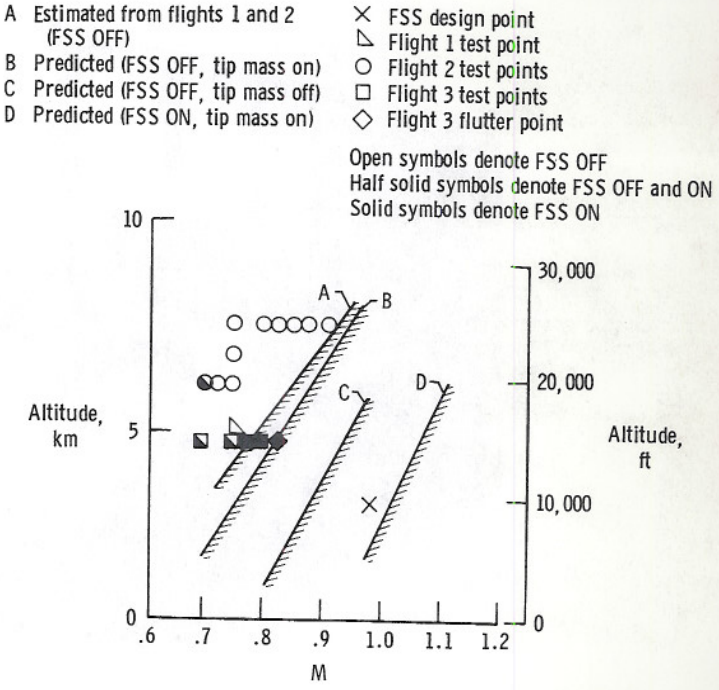

Figure 8. Flight envelope of the ARW-1 showing predicted flutter boundaries and flight-test points.

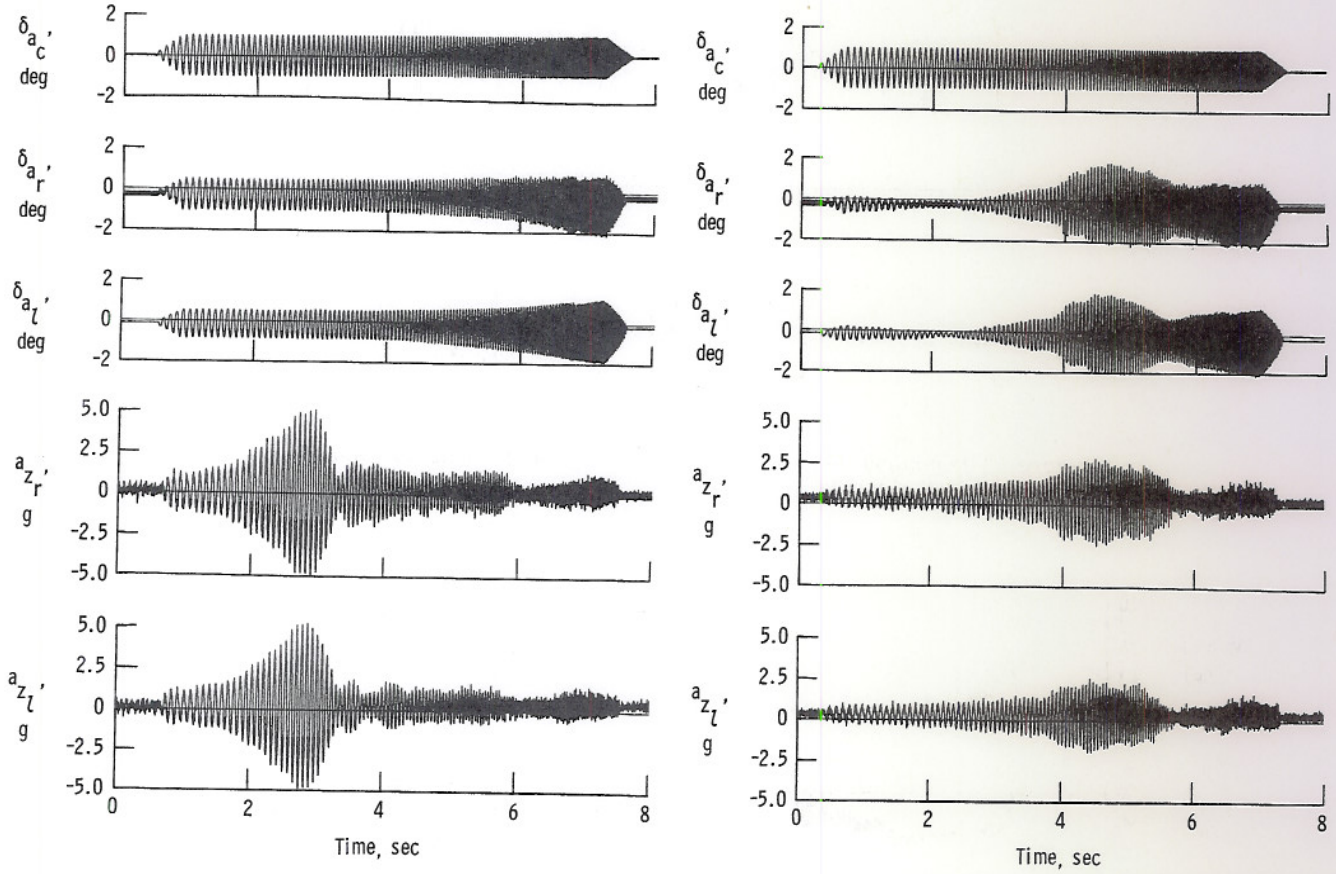

(a) FSS OFF.

(b) FSS ON.

Figure 9. Response to symmetrical frequency sweep excitation at M = 0.74 and H = 4.57 km (15,000 ft) during flight 3.

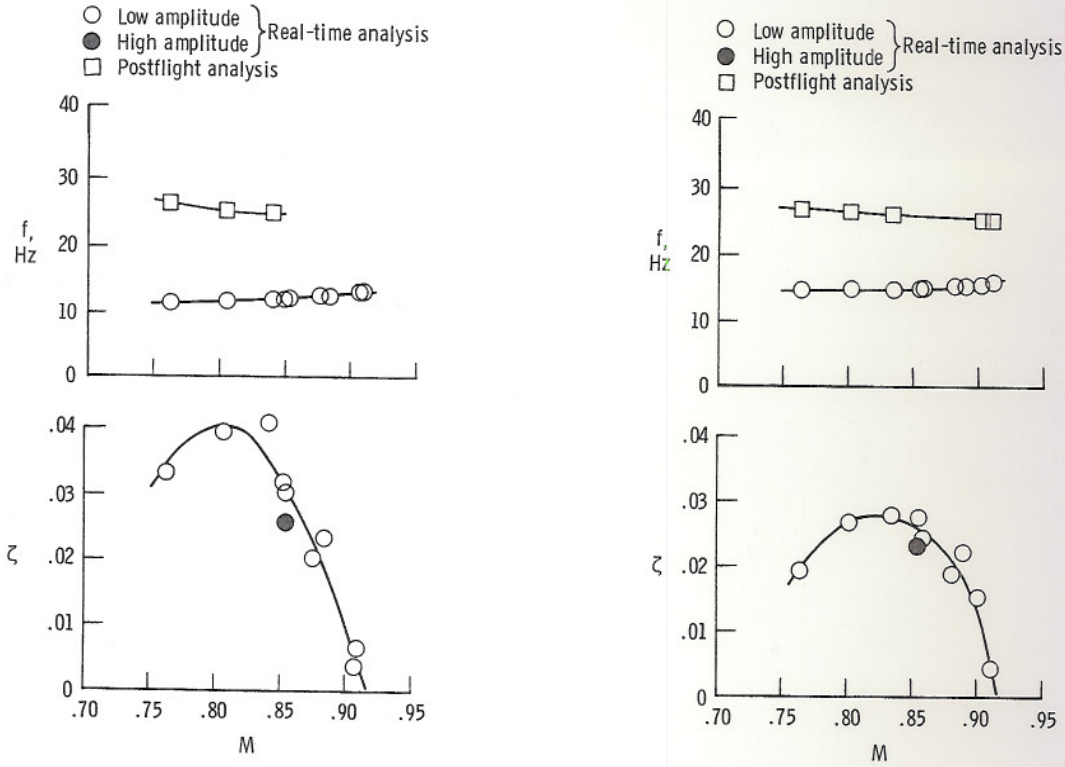

(a) Symmetric.

(b) Antisymmetric.

Figure 10. Bending-mode frequency and damping at H = 7.62 km (25,000 ft).

Figure 11. Comparison of predicted and measured antisymmetrical root loci versus Mach number at H = 4.57 km (15,000 ft).

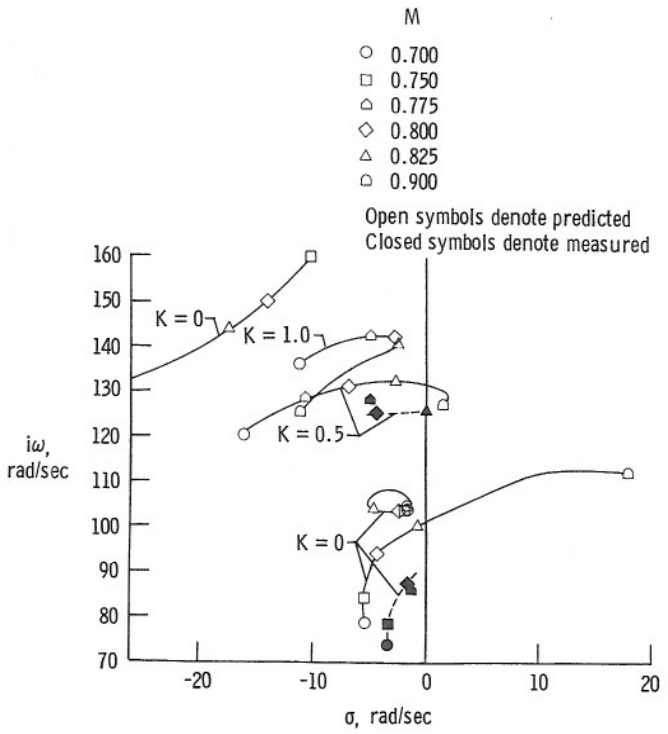

Figure 12. Comparison of predicted and measured symmetrical root loci versus Mach number at H = 4.57 km (15,000 ft).

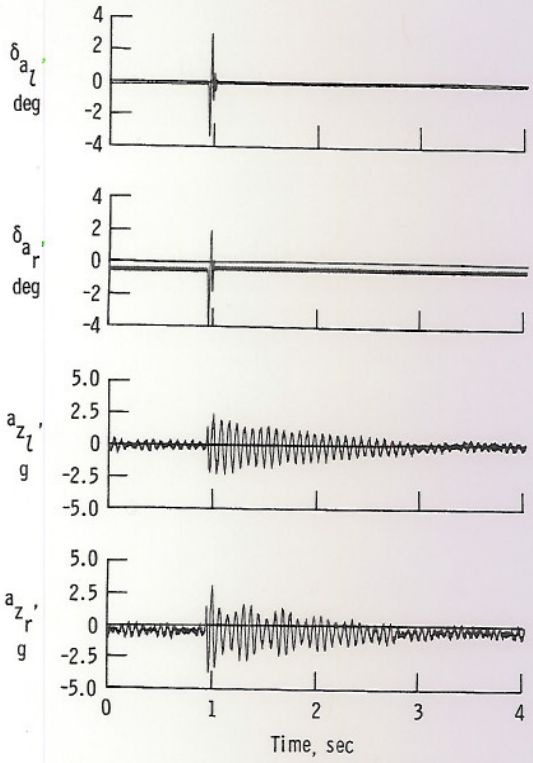

Figure 13. Symmetric, open-loop response to pulse excitation at M = 0.907 and H = 7.62 km (25,000 ft).

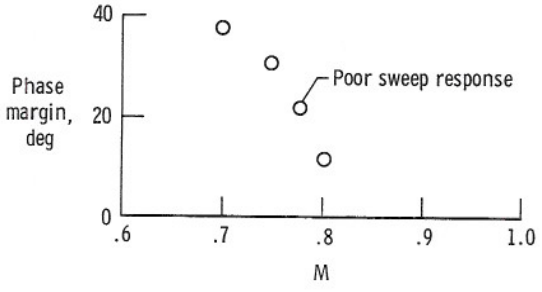

(a) Symmetric.

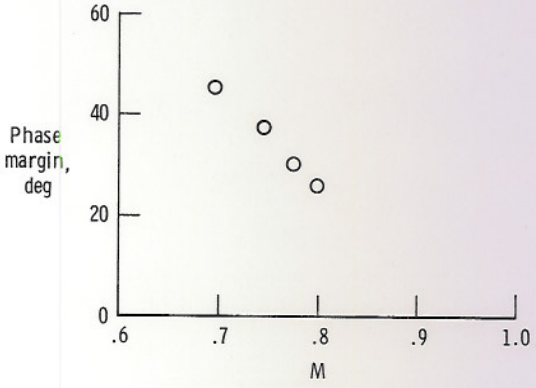

(b) Antisymmetric.

Figure 14. Phase margins obtained from flight 3 FSS ON sweeps (H = 4.57 km (15,000 ft)).

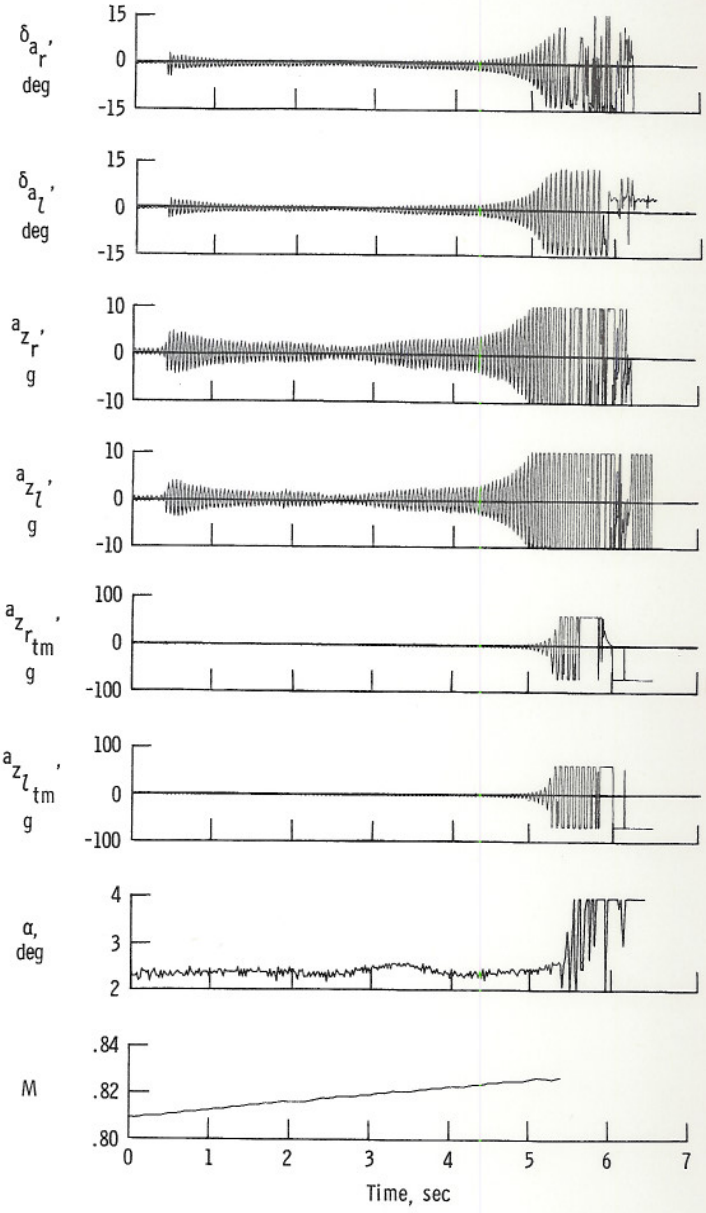

Figure 15. Response following symmetric, FSS ON pulse excitation at M ≈ 0.825 and H = 4.57 km (15,000 ft).

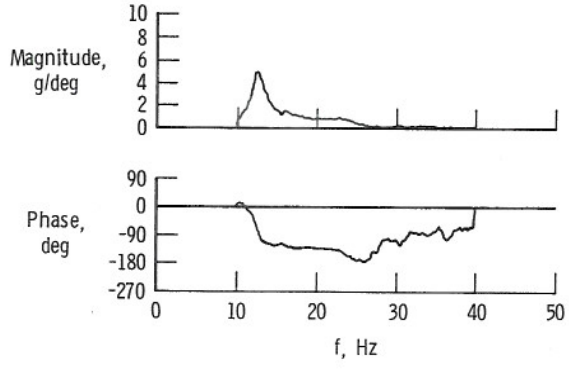

Figure 16. Smoothed transfer-function estimate of a_z due to δ_a for a symmetrical frequency sweep using a symmetrical exponential window: M = 0.74 and H = 4.57 km (15,000 ft).

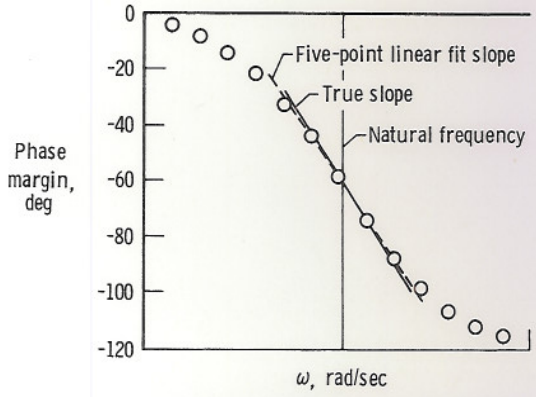

Figure 17. Phase-curve slope determination (five-point linear least-squares fit of slope).

1. Report No.	2. Government Accession No.	3. Recipient's Catalog No.
NASA TM-84901		

4. Title and Subtitle	5. Report Date
Real-Time Flutter Analysis of an Active Flutter-Suppression System on a Remotely Piloted Research Aircraft	January 1983
	6. Performing Organization Code: RTOP 505-33-41
7. Author(s): Glenn B. Gilyard and John W. Edwards	8. Performing Organization Report No.
9. Performing Organization Name and Address: Ames Research Center, Dryden Flight Research Facility, P.O. Box 273, Edwards, California 93523	10. Work Unit No.
	11. Contract or Grant No.
12. Sponsoring Agency Name and Address: National Aeronautics and Space Administration, Washington, D.C. 20546	13. Type of Report and Period Covered: Technical Memorandum
	14. Sponsoring Agency Code

15. Supplementary Notes

This paper was presented at the AGARD Flight Mechanics Panel Symposium held at Çeşme, Turkey, October 11-14, 1982

16. Abstract

Flight flutter-test results of the first aeroelastic research wing (ARW-1) of NASA's drones for aerodynamic and structural testing (DAST) program are presented. The flight-test operation and the implementation of the active flutter-suppression system are described. The software techniques used to obtain real-time damping estimates and the actual flutter testing procedure are also described in detail. Real-time analysis of fast-frequency aileron excitation sweeps provided reliable damping estimates. The open-loop flutter boundary was well defined at two altitudes; a maximum Mach number of 0.91 was obtained. Both open-loop and closed-loop data have been of exceptionally high quality. Although the flutter-suppression system provided augmented damping at speeds below the flutter boundary, an error in the implementation of the system resulted in the system being less stable than predicted. The vehicle encountered system-on flutter shortly after crossing the open-loop flutter boundary on the third flight and was lost. The aircraft has been rebuilt, and initial testing is scheduled for the fall of 1982. Changes made in real-time test techniques are included.

17. Key Words (Suggested by Author(s))	18. Distribution Statement
Flutter Active controls Flight test	Unclassified—Unlimited STAR category 05

19. Security Classif. (of this report)	20. Security Classif. (of this page)	21. No. of Pages	22. Price*
Unclassified	Unclassified	16	A02

*For sale by the National Technical Information Service, Springfield, Virginia 22161